Chemical Geology 477 (2018) 112–122

Contents lists available at ScienceDirect

Chemical Geology

journal homepage: www.elsevier.com/locate/chemgeo

Rapid formation of eclogites during a nearly closed ocean: Revisiting the Pianshishan eclogite in Qiangtang, central Tibetan Plateau

Wei Dan[a,b,c,*], Qiang Wang[a,b,d], William M. White[c], Xiu-Zheng Zhang[a], Gong-Jian Tang[a,b], Zi-Qi Jiang[e], Lu-Lu Hao[a], Quan Ou[a]

[a] State Key Laboratory of Isotope Geochemistry, Guangzhou Institute of Geochemistry, Chinese Academy of Sciences, Guangzhou 510640, China
[b] CAS Center for Excellence in Tibetan Plateau Earth Science, Beijing 100101, China
[c] Department of Earth and Atmospheric Sciences, Cornell University, Ithaca, NY 14853, USA
[d] College of Earth Sciences, University of Chinese Academy of Sciences, Beijing 10069, China
[e] School of Earth Sciences, Guilin University of Technology, Guilin 541004, China

ARTICLE INFO

Editor: K. Mezger

Keywords:
Eclogite
Geochronology
Oceanic island basalts
Petit-spot
Qiangtang
Paleo-Tethys

ABSTRACT

The Pianshishan eclogites discovered in central Qiangtang are a key piece of evidence constraining the main suture of the Paleo-Tethys Ocean in Tibet. Based on the eclogite-facies metamorphic inclusions found in them, a previous study interpreted the zircon grains as metamorphic in origin, although their catholuminescence images were similar to zircons of igneous origin. Distinguishing metamorphic from igneous zircons can be difficult, however, especially in high-pressure metamorphic rocks. In this study, we report new SIMS zircon U-Pb dates along with zircon O isotope and trace element analyses, to constrain the origin of these zircons and the interpretation of zircon dates. Twenty-five of 26 zircons analyzed from three samples yielded zircon U-Pb dates ranging from 239 to 236 Ma with an average of 238 ± 1 Ma. The zircon rare earth element (REE) patterns are characterized by positive Ce and negative Eu anomalies, strongly indicating an igneous origin. This interpretation is also supported by the high Ti-in-zircon temperatures (> 700 °C) and depleted mantle-like zircon O isotope ratios (5.15 ± 0.57‰, 2SD). Thus, we conclude that the protoliths of the Pianshishan eclogites were generated at ~238 Ma. Their geochemistry is similar to the oceanic island basalts (OIB), and they were probably generated by small extents partial melting of enriched oceanic asthenospheric mantle within the garnet stability field and emplaced or erupted as a seamount in the Paleo-Tethys Ocean. We infer the age of eclogite-facies metamorphism to be ~233 Ma based on previously reported Lu-Hf isochron ages, and that this metamorphism marks the collision between the Southern and Northern Qiangtang terranes. Thus, metamorphism of the eclogites occurred within 5 My of protolith generation and exhumation occurred only 13 to 19 My later, based on the $^{40}Ar/^{39}Ar$ dates of 220–214 Ma. The time between protolith generation and exhumation was thus < 24 My. This rare rapid evolution may be due to the protoliths having formed as a "petit-spot" seamount in response to outer rise flexure as the Paleo-Tethys Ocean entered the Longmu Co-Shuanghu subduction zone.

1. Introduction

Eclogites, mostly found in orogenic belts, signal the existence of a subduction zone and can provide important information about metamorphic processes during continent collision. The Pianshishan eclogites discovered in the Qiangtang Terrane of Tibet provide direct evidence to support an in-situ suture (the Longmu Co-Shuanghu Suture between the North and South Qiangtang terranes) related to closure of the Paleo-Tethys Ocean in Tibet (Li et al., 2006a; Zhang et al., 2006a). Based on the eclogite-facies metamorphic inclusions found in zircons from these eclogites, Zhai et al. (2011a) interpreted the zircon dates as representing the timing of eclogite-facies metamorphism. However, the zircon grains are similar to igneous ones in cathodoluminescence (CL) images; furthermore, some studies have shown that eclogite-facies metamorphic inclusions can be introduced along cracks into primary zircons during later metamorphism or exhumation (e.g., Gebauer et al., 1997; Zhang et al., 2009). Thus, additional study is needed to determine whether the zircons are metamorphic or igneous and thus whether their ages date protolith formation or subsequent metamorphism. This is in turn of importance in constraining the evolution of the Qiangtang Terrane and closure of the Paleo-Tethys Ocean.

Distinguishing metamorphic from igneous zircons is generally done

* Corresponding author at: State Key Laboratory of Isotope Geochemistry, Guangzhou Institute of Geochemistry, Chinese Academy of Sciences, Guangzhou 510640, China.
E-mail address: danwei@gig.ac.cn (W. Dan).

https://doi.org/10.1016/j.chemgeo.2017.12.012
Received 7 August 2017; Received in revised form 10 December 2017; Accepted 18 December 2017
Available online 20 December 2017
0009-2541/

based on CL imaging and Th/U ratios (Hoskin and Schaltegger, 2003; Corfu et al., 2003). Although these tools are usually effective in ascertaining the igneous origin of zircons from magmatic rocks with no metamorphism overprint, results can be ambiguous when both igneous and metamorphic zircons are present in high-grade metamorphic rocks. During the past few years, many studies have shown that zircon trace element abundances can provide a direct link between zircon formation and metamorphic conditions (e.g., Möller et al., 2003; Chen et al., 2010; Cheng et al., 2015). Metamorphic zircons grown during the eclogite-facies metamorphism exhibit distinctly different REE patterns from igneous zircons due to the tendency for heavy REE (HREE) to strongly concentrate in garnet in metamorphic zircons (e.g., Chen et al., 2010; Cheng et al., 2015). Additionally, plagioclase, which concentrates Eu, is not stable under the high-pressure conditions of eclogite-facies metamorphism and consequently metamorphic zircons do not develop negative Eu anomalies whereas zircons grown in magmas precipitating plagioclase commonly do.

In this study, comprehensive analyses of in situ zircon U–Pb–O isotope ratios and trace element abundances were carried out on the Pianshishan eclogite in central Qiangtang, Tibet. These new data are used to distinguish igneous and metamorphic zircons and reinterpret the zircon U-Pb dates. Then, the zircon U-Pb ages, combined with the whole-rock geochemistry, Sr-Nd isotopes and available data from the literature, provide new insights into the origin of the eclogite protoliths and the geodynamics of the closure of the Paleo-Tethys Ocean in Tibet.

2. Tectonic setting

The Tibetan Plateau consists mainly of the Songpan-Ganze, Qiangtang and Lhasa terranes from north to south (Fig. 1a; Yin and Harrison, 2000). The Qiangtang Terrane is divided into the North Qiangtang Terrane (NQT) and South Qiangtang Terrane (SQT) by the Longmu Co-Shuanghu suture (LSS) (e.g., Li, 1987; Zhang et al., 2006a, 2006b; Zhai et al., 2011a; Zhang X.Z. et al., 2016). From the Carboniferous into the Triassic, the southern part of the NQT underwent several episodes of subduction-related magmatism related to the subduction of the Paleo-Tethys oceanic plate (Yang et al., 2014; Jiang et al., 2015). In contrast, the northern part of the SQT was a passive continental margin from the Late Paleozoic to the Middle Triassic. The SQT underwent extension-related magmatism during the Early Permian, represented by the E-W oriented ~300–280 Ma mafic dike swarms associated with rifting of the SQT from northern Gondwana (Zhai et al., 2013). Subsequently, the SQT was carried northward along with the rest of the Cimmerian continental fragment as the Neo-Tethys Ocean opened behind it during the Permian and Triassic (Metcalfe, 1996, 2013). The SQT was accreted to the NQT as the Longmu Co-Shuanghu Tethys or Paleo-Tethys Ocean closed in the Late Triassic, an event supported by both the 230–209 Ma $^{40}Ar/^{39}Ar$ age of high-pressure metamorphic rocks and the 225–205 Ma post-collisional bimodal magmatic rocks along the LSS (Wu et al., 2015 and references therein).

Eclogites were discovered in three locations in the central Qiangtang terrane (Fig. 1b). We focus here on the first discovered and most famous of these eclogites, located in the Pianshishan area (Li et al., 2006a; Zhang et al., 2006a; Zhai et al., 2011a) and previously named the Gemu eclogite. The Pianshishan eclogites are the largest in Qiangtang with an area over tens of km^2, and are found within ductile shear zones. They occur as dikes or massive blocks in the garnet-phengite schists or rare marbles in the Pianshishan area. Previous studies have produced a range of estimated ages and P-T metamorphic conditions for the eclogites. Li et al. (2006a, 2006b) obtained phengite $^{40}Ar/^{39}Ar$ ages of 220 Ma, and estimated the temperature and pressure of metamorphism to be 349–464 °C and 1.56–2.35 GPa. Zhang et al. (2006a) estimated somewhat higher peak metamorphic conditions, 482–625 °C and 2.0–2.5 GPa. Pullen et al. (2008) obtained Lu-Hf isochron dates of 244 ± 11 Ma and 233 ± 13 Ma, which they interpreted as the timing of eclogite-facies metamorphism. Zhai et al. (2011a) obtained U-Pb zircon dates from 237 ± 3 Ma to 230 ± 4 Ma, which they also interpreted as the age of peak metamorphism and estimated those conditions to be 410–460 °C and 2.0–2.5 GPa. They also obtained a $^{40}Ar/^{39}Ar$ date of 214.1 ± 1.8 Ma on phengites from the eclogites, and interpreted these dates as well as the $^{40}Ar/^{39}Ar$ dates of Li et al. (2006b) as the cooling age of exhumation to the greenschist-facies.

Two other eclogites, Gangma Co and Guoganjianianshan, are located near an ophiolitic mélange, and occurred as lenses or blocks ranging from 50 cm to 50 m within garnet-phengite (mica) schists (Dong and Li, 2009; Zhang et al., 2010; Zhai et al., 2011a). They underwent peak eclogite-facies metamorphic conditions similar to those of the Pianshishan eclogites, but differ from them geochemically (Dong

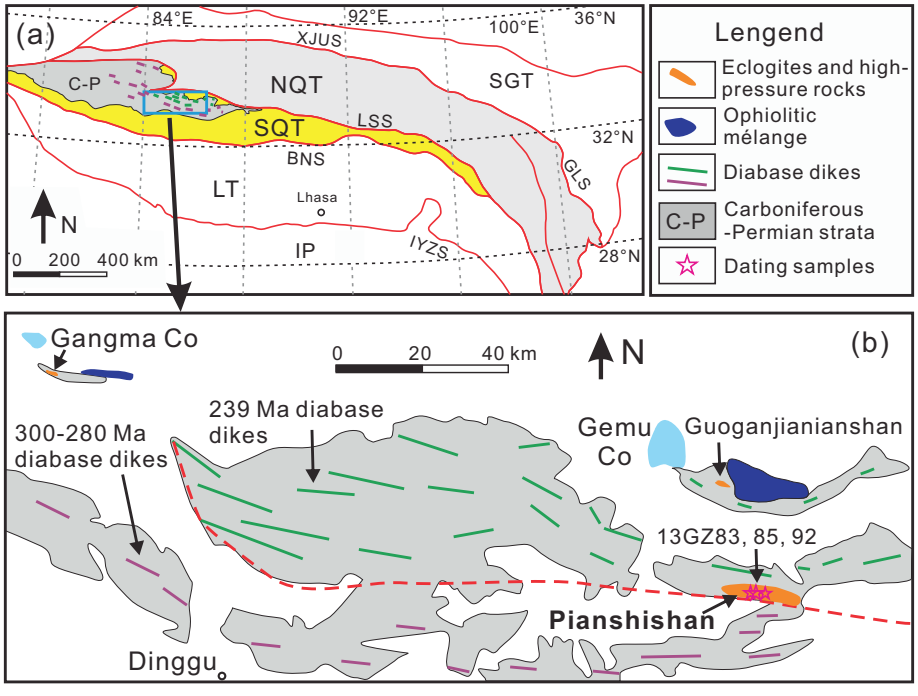

Fig. 1. Simplified geological map of the Qiangtang eclogites and mafic dikes in the Tibet. (a) Terranes: IP, India Plate; LT, Lhasa Terrane; NQT, North Qiangtang-Changdu Terrane; SGT, Songpan-Ganze Terrane; SQT, South Qiangtang Terrane. Sutures: BNS, Bangong-Nujiang suture; GLS, Ganze-Litang suture; IYZS, Indus-Yarlung Zangbo suture; LSS, Longmu Co-Shuanghu suture; XJUS, Xijin Ulan suture. The dashed red line divides the 239 Ma (Dan et al., under review) from the ~300–280 Ma (Zhai et al., 2013) mafic dike swarms. (For interpretation of the references to colour in this figure legend, the reader is referred to the web version of this article.)

and Li, 2009; Zhai et al., 2011b). $^{40}Ar/^{39}Ar$ dates of 242 Ma (Zhang et al., 2010) and 220 Ma (Zhai et al., 2011a), interpreted as the age of exhumation to the blueschist-facies, were obtained from the Guoganjianianshan garnet-phengite schists and Gangma Co eclogites, respectively.

3. Analytical methods

3.1. Cathodoluminescence images

CL images were collected using the Gatan Mono CL3 electron probe microanalyzer at the State Key Laboratory of Isotope Geochemistry, Guangzhou Institute of Geochemistry, Chinese Academy of Sciences (SKLaBIG GIGCAS). An accelerating voltage of 10 kV was used and a sample current was 2 nA.

3.2. Zircon U-Pb dating, O isotope and trace element analyses

Measurements of U, Th and Pb isotopic ratios were conducted using the Cameca IMS-1280 Secondary Ion Mass Spectrometer (SIMS) at the Institute of Geology and Geophysics, Chinese Academy of Sciences (IGG-CAS), Beijing. The analytical procedures were similar to those described by Li et al. (2009). A long-term uncertainty of 1.5% (1σ RSD) for $^{206}Pb/^{238}U$ measurements of standard zircons was propagated to the unknowns (Li Q.L. et al., 2010) in the uncertainties listed in Table 1, despite a few individual $^{206}Pb/^{238}U$ measured errors during the course of this study being smaller: 1% (1σ RSD) or less. Uncertainties on individual analyses in Table 1 are reported at a 1σ level. Mean dates for pooled U/Pb analyses are quoted with 2σ and/or 95% confidence intervals.

Zircon O isotope ratios were measured in the same Cameca IMS-1280 SIMS at IGG-CAS, following standard procedures (Li et al., 2010a; Tang et al., 2015). The measured oxygen isotopic data were corrected for instrumental mass fractionation using the Penglai zircon standard ($\delta^{18}O_{VSMOW}$ = 5.3‰) (Li et al., 2010b). The internal precision of a single analysis generally was better than 0.40‰ (2σ standard error) for the $^{18}O/^{16}O$ ratio. The external precision, measured by the reproducibility of repeated analyses of Penglai standard, is 0.41‰ (2SD, n = 20). Eight measurements of the Qinghu zircon standard, used in many Chinese laboratories, during the course of this study yielded a weighted mean of $\delta^{18}O$ = 5.51 ± 0.35‰ (2SD), which is within error of the reported value of 5.4 ± 0.2‰ (Li et al., 2013).

Zircon trace element abundances were measured using an Agilent 7500a ICP-MS with an attached 193 nm excimer ArF laser-ablation system (GeoLas Plus) at IGG-CAS with a laser spot size of 35 μm. The analytical procedures are similar to those described by Xie et al. (2008). Trace element concentrations were calibrated by using ^{29}Si as internal calibration and NIST SRM610 as reference material. The precision and accuracy of the zircon 91500 (Wiedenbeck et al., 2004) analyses are 3–13% for most elements at the ppm concentration level.

3.3. Whole-rock geochemical analyses

Whole-rock geochemical analyses, including major and trace elements, and Sr-Nd isotopes, were carried out at SKLaBIG GIGCAS. Rock samples crushed to ~200-mesh size were used for geochemical analyses. Major element oxides were analyzed on fused glass beads using a Rigaku RIX 2000 X-ray fluorescence spectrometer. Calibration lines used in quantification were produced by bivariate regression of data from 36 reference materials encompassing a wide range of silicate compositions (Li et al., 2005). Analytical uncertainties are between 1% and 5%. Trace elements were analyzed using an Agilent 7500a ICP-MS. Analytical procedures were similar to those described by Li et al. (2000). An internal standard solution containing the single element Rh was used to monitor signal drift during counting. A set of USGS and Chinese national rock standards, including BHVO-2, AGV-2, W-2a, GSR-

Table 1
SIMS zircon U-Pb dating results for the Pianshishan eclogites.

Sample spot	U	Th	Th/U	f_{206}%	$^{207}Pb/^{206}Pb$	± σ	$^{207}Pb/^{235}U$	± σ	$^{206}Pb/^{238}U$	± σ	ρ	$^{207}Pb/^{206}Pb$	± σ	$^{207}Pb/^{235}U$	± σ	$^{206}Pb/^{238}U$	± σ
	ppm	ppm			%		%		%								
Sample 13GZ83-1 33°24′27″N, 86°01′09″E																	
13GZ83-1@1	1097	1645	1.50	0.05	0.0505	0.72	0.255	1.68	0.0366	1.52	0.904	219.9	16.5	230.8	3.5	231.9	3.5
13GZ83-1@2	783	847	1.08	0.06	0.0510	0.68	0.261	1.65	0.0370	1.51	0.912	241.9	15.6	235.1	3.5	234.4	3.5
13GZ83-1@3	461	693	1.50	0.10	0.0508	1.23	0.265	1.94	0.0378	1.50	0.774	231.8	28.2	238.5	4.1	239.1	3.5
13GZ83-1@4	1565	2115	1.35	0.05	0.0501	0.49	0.261	1.59	0.0378	1.51	0.951	198.2	11.4	235.3	3.3	239.0	3.6
Sample 13GZ85-1 33°24′27″N, 86°01′09″E																	
13GZ85-1@1	367	446	1.22	0.15	0.0515	1.23	0.273	1.94	0.0384	1.50	0.773	264.6	28.0	245.2	4.2	243.2	3.6
13GZ85-1@2	931	429	0.46	0.17	0.0507	1.04	0.260	1.85	0.0372	1.53	0.827	225.1	23.8	234.6	3.9	235.5	3.5
13GZ85-1@3	540	729	1.35	0.10	0.0515	0.98	0.271	1.79	0.0381	1.51	0.839	263.2	22.3	243.2	3.9	241.1	3.6
13GZ85-1@4	456	637	1.40	0.09	0.0504	1.17	0.262	1.91	0.0377	1.51	0.789	213.8	27.0	236.4	4.0	238.7	3.5
13GZ85-1@5	1320	271	0.21	0.10	0.0505	0.68	0.255	1.72	0.0366	1.58	0.918	217.7	15.7	230.4	3.6	231.6	3.6
13GZ85-1@6	303	173	0.57	0.61	0.0488	2.48	0.252	2.93	0.0375	1.55	0.531	137.9	57.3	228.5	6.0	237.4	3.6
13GZ85-1@7	583	782	1.34	0.21	0.0514	1.24	0.276	1.95	0.0389	1.50	0.771	259.9	28.3	247.1	4.3	245.8	3.6
13GZ85-1@8	455	621	1.36	0.25	0.0510	1.33	0.263	2.03	0.0373	1.53	0.755	241.9	30.4	236.7	4.3	236.2	3.6
13GZ85-1@9	181	152	0.84	0.55	0.0533	1.51	0.276	2.14	0.0376	1.52	0.708	340.2	33.9	247.5	4.7	237.8	3.5
Sample 13GZ92-2 33°24′27″N, 86°01′09″E																	
13GZ92-2@1	714	1086	1.52	0.38	0.0511	1.93	0.262	2.45	0.0372	1.51	0.616	247.0	43.9	236.6	5.2	235.6	3.5
13GZ92-2@2	1376	1684	1.22	0.05	0.0510	0.52	0.263	1.59	0.0374	1.50	0.946	238.9	11.9	236.8	3.4	236.6	3.5
13GZ92-2@3	1750	2709	1.55	0.34	0.0498	0.96	0.262	1.78	0.0382	1.50	0.844	187.9	22.1	236.6	3.8	241.6	3.6
13GZ92-2@4	1244	2360	1.90	0.26	0.0518	0.55	0.271	1.60	0.0380	1.51	0.940	277.0	12.5	243.7	3.5	240.2	3.6
13GZ92-2@5	920	1147	1.25	0.05	0.0509	0.76	0.260	1.68	0.0370	1.50	0.893	234.9	17.4	234.5	3.5	234.4	3.5
13GZ92-2@6	927	1643	1.77	0.04	0.0515	0.69	0.262	1.67	0.0369	1.52	0.909	265.2	15.9	236.4	3.5	233.5	3.5
13GZ92-2@7	1050	1262	1.20	0.00	0.0503	0.59	0.260	1.62	0.0376	1.51	0.931	206.6	13.7	235.1	3.4	237.9	3.5
13GZ92-2@8	516	672	1.30	0.09	0.0502	0.97	0.257	1.79	0.0370	1.51	0.841	206.1	22.4	231.9	3.7	234.5	3.5
13GZ92-2@9	1404	1878	1.34	0.07	0.0507	0.51	0.266	1.59	0.0380	1.50	0.948	226.3	11.7	239.3	3.4	240.7	3.6
13GZ92-2@10	5333	11,818	2.22	0.18	0.0509	0.54	0.270	1.60	0.0384	1.50	0.940	236.8	12.5	242.4	3.5	243.0	3.6
13GZ92-2@11	1604	2517	1.57	0.14	0.0502	0.67	0.256	1.65	0.0370	1.51	0.915	202.4	15.4	231.1	3.4	233.9	3.5
13GZ92-2@12	1484	2514	1.69	0.05	0.0504	0.49	0.260	1.61	0.0375	1.53	0.952	213.0	11.3	235.0	3.4	237.2	3.6
13GZ92-2@13	2374	4719	1.99	0.51	0.0497	0.81	0.240	1.73	0.0350	1.53	0.884	182.9	18.7	218.3	3.4	221.6	3.3

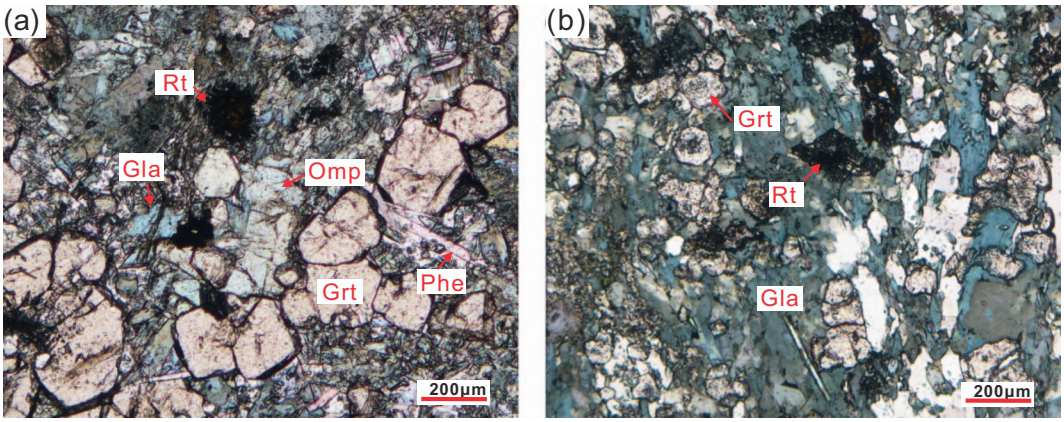

Fig. 2. Photomicrographs showing mineral assemblage in the Pianshishan eclogites. The eclogites collected from the inner and outer part of massive blocks commonly preserved eclogites-facies (peak stage) (a) and blueschist-facies (retrograded stage) (b) metamorphic mineral assemblages, respectively. Mineral abbreviations: Grt, garnet; Omp, Omphacite; Phe, phengite; Gla, glaucophane; Rt, rutile.

1 and GSR-2 were chosen for calibration. Analytical precision is typically better than 5%. Sr–Nd isotopic compositions were determined using a Micromass Isoprobe multi-collector ICP-MS. Analytical procedures are similar to those described in Li et al. (2004). All measured Nd and Sr isotope ratios were normalized to $^{146}Nd/^{144}Nd = 0.7219$ and $^{86}Sr/^{88}Sr = 0.1194$, respectively. The measured $^{87}Sr/^{86}Sr$ ratio of the NBS 987 standard and $^{143}Nd/^{144}Nd$ ratio of the JNdi-1 standard were 0.710274 ± 18 (n = 11, 2σ) and 0.512093 ± 11 (n = 11, 2σ), respectively. The reported Sr and Nd isotope values were adjusted to 0.710248 and 0.512115, respectively.

4. Results

4.1. Zircon U-Pb, O isotopes and trace elements

Three Pianshishan eclogite samples (Fig. 2) were selected for SIMS U-Pb zircon dating. Single spot analyses were conducted on total of 26 individual grains. Zircons separated from these rocks are similar to those of the previous study of Zhai et al. (2011a). They are mostly euhedral to subhedral, spherical or short prismatic crystals with banded zoning in CL images (Fig. 3) and have high Th, U contents and Th/U ratios (0.21–2.22, mostly > 1) (Table 1).

Four grains from sample 13GZ83-1 and nine grains from sample 13GZ 85-1 give weighted $^{206}Pb/^{238}U$ dates of 236 ± 3 Ma and 239 ± 3 Ma, respectively (Fig. 4). Twelve of thirteen grains from sample 13GZ92-1 give a weighted $^{206}Pb/^{238}U$ date of 237 ± 2 Ma. One grain produced a younger $^{206}Pb/^{238}U$ date of 222 ± 3 Ma, similar to the ~220 Ma $^{40}Ar/^{39}Ar$ dates (Li et al., 2006b), probably caused by Pb loss during later metamorphism. This grain plots slightly above the Concordia line, possibly caused by its higher common lead (f_{206} = 0.51%), compared with the remaining spots with f_{206} of 0–0.38% (Table 1). Together, these analyses define a weighted $^{206}Pb/^{238}U$ date of 238 ± 1 Ma (Fig. 4d), which will be used in the flowing discussion.

Measured zircon $\delta^{18}O$ values for one eclogite sample (13GZ92-1) show a limited range of 4.7–5.5‰ (Table 2; Fig. 5a), with an averaged value of 5.15 ± 0.57‰ (2SD), which is similar to or slightly less than the depleted mantle zircon value of 5.3 ± 0.6‰ of Valley et al. (1998).

Trace element analyses of the zircon grains were conducted subsequent to the U-Pb-O isotope analyses. The REE patterns are characterized by positive Ce and negative Eu anomalies as well as HREE enrichment (Fig. 5b). Most Ti contents are very high, up to 1390 ppm (Table 3), significantly higher than the Ti contents (< 30 ppm) in zircon from basaltic magmas (Fu et al., 2008), and most probably as a result of inclusions in the zircons (Zhai et al., 2011a). Thus, analyses

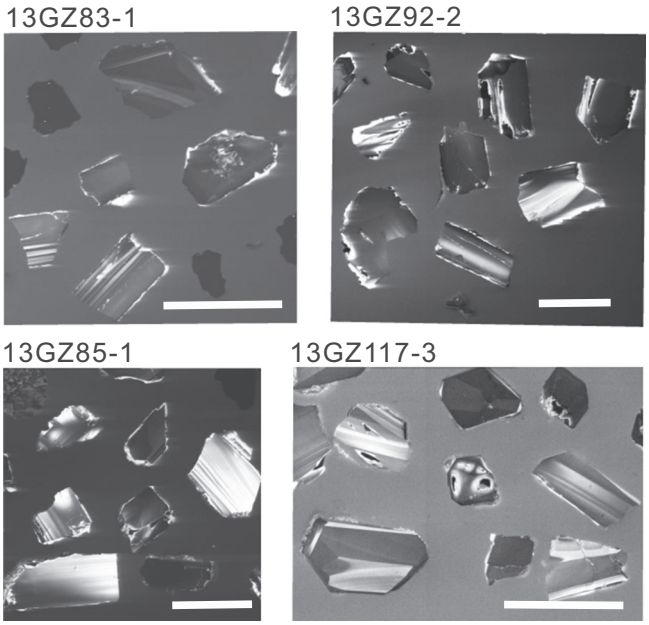

Fig. 3. CL images of representative zircons subjected to in situ analyses. The white scale bars are 100 μm long. Sample 13GZ117-3 is from the 239 Ma mafic dikes (Dan et al., under review). The zircon grains from the eclogites and mafic dikes show similar CL images.

with Ti > 30 ppm were excluded from temperature calculations. The remaining grains yielded Ti contents of 7.6–28.8 ppm, consistent with a basaltic origin (Fu et al., 2008), and the calculated temperatures based on the Ti-in-zircon geothermometer (Ferry and Watson, 2007) are 721–856 °C (Table 3).

4.2. Whole-rock geochemistry

The five samples analyzed in this study show similar whole-rock geochemistry to those of the previous study of Zhai et al. (2011b). They have low SiO_2 (45.7–47.3 wt%) and Mg#'s (35.6–41.5) and high TiO_2 (4.9–5.4 wt%) and total Fe_2O_3 (16.6–18.9 wt%) contents (Table 4). They are hypersthene or quartz normative (CIPW), implying they are tholeiitic, but plot within the alkali basalt field on the total alkali-silica diagram (Fig. 6a). They also plot within the alkalic basalt field on the Zr/Ti versus Nb/Y diagram (Fig. 6b). They exhibit light REE (LREE) enrichment relative to the HREE (Fig. 6c), and show variable positive Nb, Ta, and Ti anomalies (Fig. 6d). Positive rather than negative Ta and

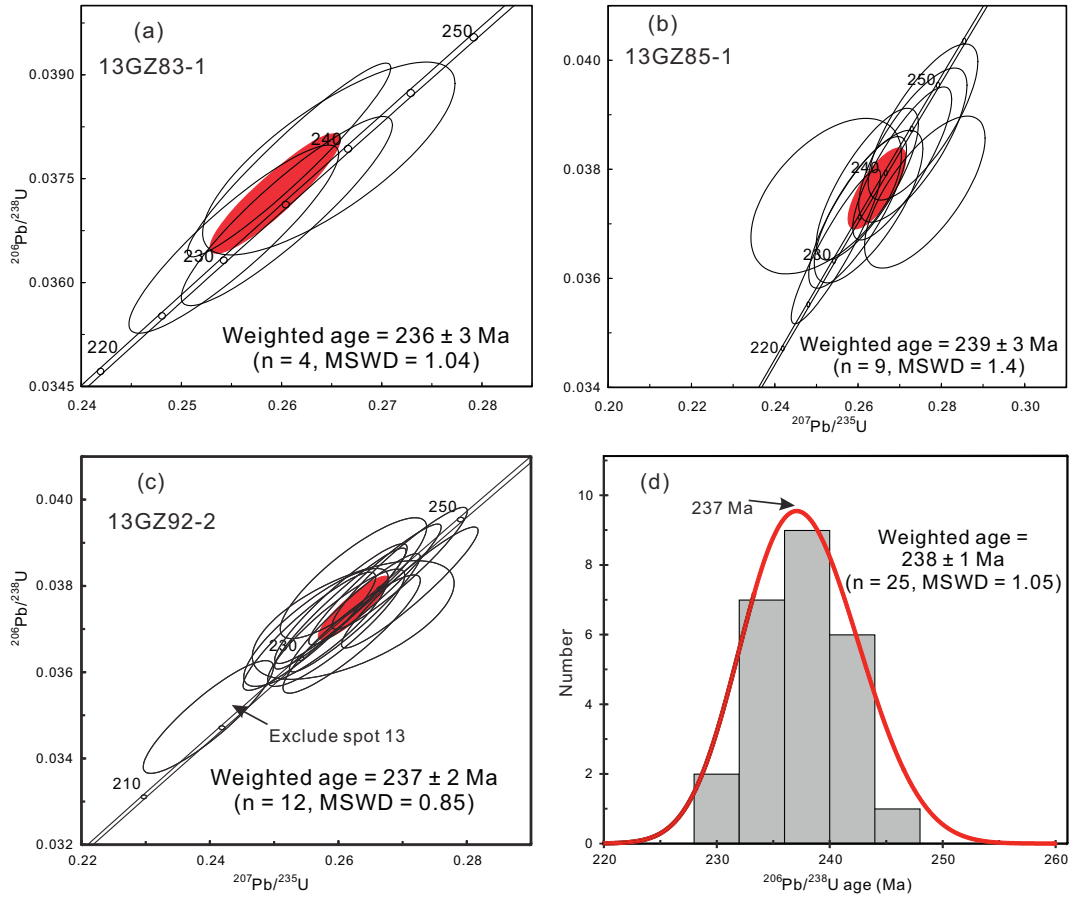

Fig. 4. SIMS Zircon U-Pb ages for the Pianshishan eclogites. a, b, c. Concordia diagrams of for zircons from the three samples. d, Histogram and probability function of SIMS zircon U-Pb dates for the Pianshishan eclogites.

Table 2
SIMS zircon O isotope results for the Pianshishan eclogites.

Sample spot	$\delta^{18}O$	2σ
13GZ92-2@1	5.47	0.40
13GZ92-2@2	5.25	0.16
13GZ92-2@3	4.94	0.32
13GZ92-2@4	4.71	0.28
13GZ92-2@5	5.24	0.35
13GZ92-2@6	4.98	0.31
13GZ92-2@7	5.46	0.36

Nb anomalies indicate that they were not generated in a supra-subduction or island arc environment nor had they assimilated continental crust.

Two samples have depleted Nd-Sr isotopic signatures ($\varepsilon_{Nd}(t)$ = +4.7 to +5.2 and $(^{87}Sr/^{86}Sr)_i$ = 0.7042 to 0.7047). These isotopic compositions plot barely within the field of modern OIB, but when that field is adjusted to what it would have been at ~238 Ma, they plot outside of it (Fig. 7). Both the trace element and isotope geochemistry of the eclogites are consistent with their protoliths being oceanic intraplate basalts, although elevated $(^{87}Sr/^{86}Sr)_i$ values indicate that they likely reacted with seawater or seawater-derived hydrothermal fluids (see Section 5.2).

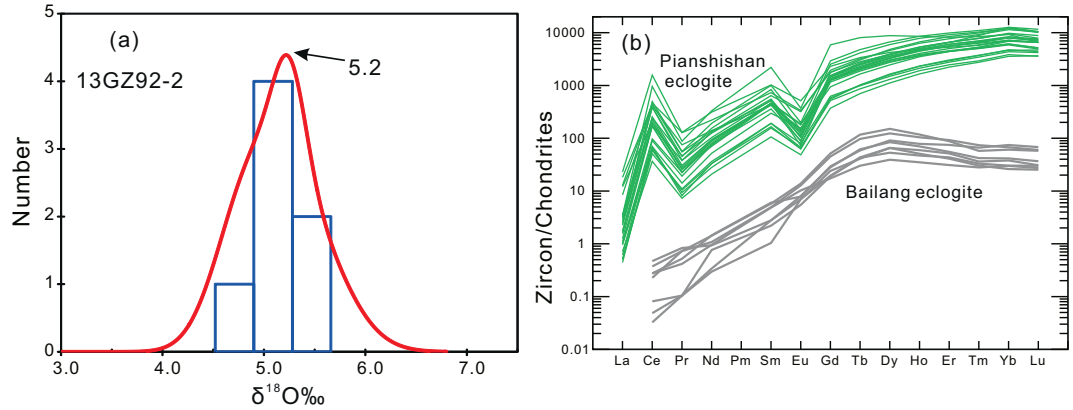

Fig. 5. (a) SIMS zircon O isotope ratios; (b) LA-ICP-MS zircon REE patterns for the Pianshishan eclogites. The normalized values are from Sun and McDonough (1989). The metamorphic zircon rims of Bailang eclogites, Tibet from Cheng et al. (2015) are shown for comparison.

Table 3
LA-ICP-MS trace element (ppm) results for the Pianshishan eclogites.

Sample spot	La	Ce	Pr	Nd	Sm	Eu	Gd	Tb	Dy	Ho	Er	Tm	Yb	Lu	Ti	T/°C[a]
13GZ83-1 01	0.54	142	2.47	33.1	68.4	7.59	303	93.2	913	278	999	179	1382	189	~~44.1~~	~~907~~
13GZ83-1 02	0.15	55.8	1.83	34.9	71.7	10.9	299	87.0	867	260	928	172	1370	186	21.6	824
13GZ83-1 04	4.35	256	7.20	66.0	65.4	8.83	281	82.8	851	271	1012	180	1443	195	~~503~~	~~1322~~
13GZ85-1 01	0.42	108	3.64	62.1	99.1	18.7	404	121.0	1182	360	1281	238	1960	266	~~46.2~~	~~913~~
13GZ85-1 02	0.23	38.5	0.90	13.2	24.1	3.92	108	32.5	335	109	411	75.5	659	91.8	~~218~~	~~1150~~
13GZ85-1 03	0.26	42.9	1.36	24.4	46.0	9.08	196	62.3	630	200	735	137	1184	169	~~31.5~~	~~866~~
13GZ85-1 04	3.07	285	12.3	147	158	30.2	477	127	1083	278	887	149	1200	167	~~210~~	~~1143~~
13GZ85-1 06	0.11	42.4	0.79	15.7	25.6	3.65	115	38.5	408	132	489	95.1	812	112	7.62	721
13GZ85-1 07	0.17	22.6	0.70	9.85	16.4	2.84	77.1	26.5	286	94.6	373	70.9	610	93.8	~~41.9~~	~~901~~
13GZ85-1 08	0.12	36.5	1.00	15.6	29.6	3.89	121	38.4	423	133	508	96.4	795	121	20.0	815
13GZ85-1 09	0.37	107	2.17	37.9	71.4	7.95	303	95.9	976	304	1099	200	1671	227	10.7	752
13GZ92-2 01	0.12	31.4	1.05	17.2	29.6	4.65	129	37.3	383	121	463	88.8	749	108	~~48.4~~	~~919~~
13GZ92-2 02	2.02	271	5.29	63.3	78.9	6.04	319	101	1012	307	1103	202	1635	201	~~366~~	~~1252~~
13GZ92-2 03	0.58	157	2.93	44.5	70.4	4.23	272	78.8	780	220	760	135	1055	131	~~1390~~	~~1596~~
13GZ92-2 04	2.89	124	2.70	44.4	65.7	6.37	258	74.6	726	212	738	129	1005	126	~~71.1~~	~~971~~
13GZ92-2 05	0.83	593	8.42	156	341	21.7	1221	305	2253	487	1371	217	1586	167	~~92.8~~	~~1009~~
13GZ92-2 06	0.39	121	2.50	41.4	69.3	5.10	270	82.4	829	255	930	167	1366	179	28.8	856
13GZ92-2 07	0.30	105	2.14	36.6	55.3	5.25	241	70.6	703	208	741	130	1044	133	24.7	838
13GZ92-2 08	5.49	970	12.3	104	113	19.6	371	106	991	288	1091	229	2173	298	~~731~~	~~1413~~
13GZ92-2 09	0.64	238	4.33	72.7	130	8.36	524	156	1526	447	1530	265	2039	258	~~54.2~~	~~934~~
13GZ92-2 10	0.77	151	4.45	59.0	85.3	6.90	316	93.8	920	265	939	162	1239	168	~~152~~	~~1087~~
13GZ92-2 11	0.24	60.0	2.17	41.6	70.4	10.5	264	77.8	765	231	836	151	1231	169	~~32.3~~	~~869~~
13GZ92-2 12	0.72	306	5.37	90.3	155	11.6	608	180	1715	487	1651	283	2158	265	~~37.9~~	~~888~~
13GZ92-2 13	0.82	242	3.66	48.5	81.1	6.09	363	115	1237	382	1410	256	2084	270	~~169~~	~~1105~~
91,500	< 0.057	2.48	< 0.044	0.25	0.46	0.24	2.48	0.90	10.6	4.58	24.5	6.27	69.9	12.4	4.59	
91,500	< 0.071	2.53	< 0.044	0.24	0.39	0.23	2.51	0.89	11.4	4.79	25.2	6.32	71.6	12.7	4.72	
91,500	< 0.074	2.60	< 0.043	0.31	0.37	0.24	1.85	0.84	10.8	4.64	24.4	6.05	68.3	12.4	6.27	
91,500	< 0.074	2.50	< 0.054	0.35	0.40	0.18	1.87	0.77	9.62	4.15	21.8	5.94	62.0	11.3	6.30	
91,500	< 0.066	2.58	< 0.045	0.33	0.42	0.21	2.35	0.82	11.3	4.65	24.5	6.24	68.4	12.2	6.62	
91,500	< 0.064	2.32	< 0.049	0.23	0.46	0.27	1.75	0.71	9.81	4.08	21.7	5.72	65.1	11.5	6.84	
91,500	< 0.058	2.35	< 0.037	0.27	0.49	0.23	1.89	0.72	9.34	4.08	21.7	5.48	63.8	11.9	7.32	
91,500	< 0.058	2.33	< 0.048	0.31	0.47	0.21	2.14	0.72	9.76	4.04	21.7	5.84	63.7	11.6	7.66	

[a] Temperatures calculated following Ferry and Watson (2007). The Ti-in-zircon thermometer is dependent on the α_{TiO2} and α_{SiO2} during crystallization, which cannot be analyzed in the eclogites. In this study, we assumed $\alpha_{TiO2} = \alpha_{SiO2}$; this and other assumptions do not significantly affect the calculated temperatures.

5. Discussion

5.1. Reinterpreting the zircon U-Pb dates

Zhai et al. (2011a) previously reported two SHRIMP zircon U-Pb dates of 230 ± 4 Ma (n = 10, MSWD = 1.6) and 237 ± 4 Ma (n = 11, MSWD = 0.64) for these eclogites. Based on a few eclogite-facies mineral inclusions (garnet, omphacite and phengite) in the zircons, Zhai et al. (2011a) interpreted these dates as dating the eclogite-facies metamorphism. However, others have shown that inclusions such as these can be introduced along cracks into primary zircons during later metamorphism or exhumation (e.g., Gebauer et al., 1997; Zhang et al., 2009). Thus, the presence of eclogite-facies inclusions is not sufficient evidence to conclude that the zircons are not primary and other data need to be considered.

The additional data we present here all favor an igneous origin for the zircons; specifically:

- First, the banded zoning in CL images, and high Th, U contents and Th/U ratios (mostly > 1) of the zircon grains are consistent with zircons crystallized from mafic magmas (Fig. 3; Hoskin and Schaltegger, 2003; Corfu et al., 2003; Wu and Zheng, 2004).
- Second, the REE patterns show positive Ce and Eu negative anomalies and no HREE depletion, characteristics of igneous zircons (Chen et al., 2010). In contrast, the metamorphic zircons grown during the eclogite-facies metamorphism, i.e., presence of garnet and absence of plagioclase, show no Eu anomalies and exhibit HREE depletion (Fig. 5b).
- Third, the calculated Ti-in-zircon temperatures are ~720–850 °C (Table 3), which are higher than the highest obtained metamorphic temperatures of 482–625 °C for the Pianshishan eclogites (Zhang et al., 2006a) and consistent with zircons crystallized from late-stage basaltic magmas (Fu et al., 2008).
- Fourth, the zircon O isotope ratios (5.15 ± 0.57‰) are similar to the depleted mantle zircon values (5.3 ± 0.6‰, Valley et al., 1998), but unlike the metamorphic zircon O isotopic ratios for eclogites, which typically exhibit a broad range from lower to higher values than the depleted mantle zircon values (e.g., Zhang et al., 2016a, 2016b).
- Finally, the estimated metamorphic temperatures are well below the zircon U-Pb closure temperatures (e.g., Lee et al., 1997), so they would not have been reset during metamorphism. Furthermore, there are no obvious metamorphic overgrowths on the zircons. This is probably due to the lack of an external fluid introduced during the eclogite-facies metamorphism, as indicated by the lack metasomatic quartz veins observed in the field.

Thus, we interpret the zircons as primary, i.e., magmatic, and the dates as crystallization ages. If the whole-rock SiO_2 and Zr concentrations are those of the bulk magma from which the protoliths formed, such a magma would not have become zircon-saturated (Boehnke et al., 2013). However, judging from the large area over which the outcrop extends, the protoliths likely formed as a dike of considerable width or lava flow of considerable depth, allowing for slow cooling and fractional crystallization producing evolved zircon-saturated residual liquids.

5.2. Protolith origin of the Pianshishan eclogites

In high-grade metamorphic rocks, the element mobility can be evaluated by plotting abundances of elements versus high field strength elements (HFSEs) including the Nb, Ta, Hf, and Zr, which are least affected during metamorphism and alteration. Elements usually considered immobile, such as the Nb, Th and REE, correlate well with the

Table 4
Major (CIPW), trace elements and Sr-Nd isotopes for the Pianshishan eclogites.

Sample	13GZ83-1	13GZ83-2	13GZ84-1	13GZ84-2	13GZ92-1	BHVO-2
Major element (%)						
SiO_2	45.73	46.23	47.33	45.62	46.94	
TiO_2	5.36	5.34	4.88	5.22	4.90	
Al_2O_3	12.87	12.72	12.20	12.17	13.16	
TFe_2O_3	16.55	16.60	17.85	18.93	16.69	
MnO	0.19	0.21	0.23	0.23	0.21	
MgO	5.34	5.22	4.49	4.92	4.77	
CaO	9.92	9.91	8.64	9.00	9.04	
Na_2O	2.59	2.50	2.84	2.69	2.80	
K_2O	0.86	0.66	0.84	0.55	0.84	
P_2O_5	0.24	0.26	0.36	0.31	0.30	
Total	99.65	99.65	99.66	99.63	99.65	
L.O·I	0.50	0.35	0.88	0.58	0.25	
CIPW norms						
Quartz			0.35			
Plagioclase	43.65	43.47	42.89	43.19	45.40	
Orthoclase	5.14	3.96	5.08	3.31	5.02	
Nepheline	0	0	0	0	0	
Diopside	22.48	21.91	19.20	19.78	18.69	
Hypersthene	9.41	16.50	19.52	16.36	16.58	
Wollastonite	0	0	0	0	0	
Olivine	5.93	0.75	0.00	3.71	1.63	
Ilmenite	10.37	10.33	9.46	10.12	9.50	
Magnetite	2.45	2.45	2.64	2.80	2.46	
Hematite	0	0	0	0	0	
Apatite	0.58	0.63	0.86	0.74	0.72	
Trace element (ppm)						
Sc	30.4	29.0	26.0	29.0	26.8	31.5
V	543	538	404	493	477	321
Cr	20.4	170	73.2	105	100	278
Co	55.4	52.0	48.8	55.6	47.3	44.0
Ni	58.0	67.1	33.7	44.9	56.1	116
Cu	102	109	305	241	363	126
Zn	144	142	171	158	144	104
Ga	24.1	23.6	24.3	23.5	24.4	21.1
Ge	3.83	2.20	4.21	4.10	2.31	3.26
Rb	19.0	14.2	17.8	12.1	17.8	9.18
Sr	373	434	373	325	379	379
Y	24.2	24.0	32.1	31.9	28.3	25.8
Zr	187	181	258	242	210	165
Nb	25.0	24.2	33.6	32.9	27.6	18.9
Cs	0.59	1.43	0.72	0.72	1.15	0.10
Ba	181	137	218	121	186	133
La	19.7	20.1	28.7	26.7	23.8	14.6
Ce	44.8	46.6	64.8	60.0	52.5	36.6
Pr	6.15	6.25	8.88	8.18	7.13	5.17
Nd	27.4	27.4	39.1	35.3	31.1	24.8
Sm	6.17	6.47	8.63	8.05	7.14	5.94
Eu	2.16	2.25	2.87	2.73	2.47	2.03
Gd	6.20	6.30	8.59	7.94	6.98	5.93
Tb	0.97	1.00	1.32	1.22	1.10	0.95
Dy	5.32	5.57	7.25	6.90	6.18	5.24
Ho	1.02	1.05	1.38	1.30	1.19	1.00
Er	2.51	2.61	3.39	3.18	2.96	2.48
Tm	0.34	0.34	0.46	0.42	0.40	0.33
Yb	1.97	2.08	2.66	2.51	2.38	1.96
Lu	0.29	0.30	0.39	0.36	0.34	0.29
Hf	5.03	4.73	6.99	6.57	5.31	4.65
Ta	1.93	1.85	2.55	2.46	2.05	1.35
Pb	2.26	2.62	2.97	2.13	3.70	2.74
Th	2.38	2.54	3.48	3.29	2.89	1.19
U	0.57	0.61	0.82	0.81	0.66	0.41
Mg#[a]	41.5	40.9	35.6	36.4	38.6	
$(La/Yb)_N$	7.20	6.95	7.75	7.64	7.20	
Sr-Nd isotopes						
$^{87}Rb/^{86}Sr$	0.1471				0.1358	
$^{87}Sr/^{86}Sr_{(m)}$	0.704662				0.705129	0.703486
1SE	0.000008				0.000008	
$^{87}Sr/^{86}Sr_{(i)}$	0.704165				0.704669	
$^{147}Sm/^{144}Nd$	0.1361				0.1388	
$^{147}Nd/^{146}Nd_{(m)}$	0.512808				0.512788	0.512988
1SE	0.000005				0.000004	

(*continued on next page*)

Table 4 (*continued*)

Sample	13GZ83-1	13GZ83-2	13GZ84-1	13GZ84-2	13GZ92-1	BHVO-2
$\varepsilon Nd_{(t)}$	5.16				4.69	

a) Parameters: $Mg^{\#} = Mg^{2+} \times 100/(Mg^{2+} + Fe^{2+})$, assuming $FeO/(FeO + Fe_2O_3) = 0.9$.

Zr (Fig. 8), but other elements, such as the Ba and Sr, do not. In addition, some of the Zhai et al. (2011b) samples show strong Ba and K anomalies in their trace element patterns (Fig. 6d), which is consistent with secondary mobility. The quartz-normative CIPW norms, indicative of tholeiitic compositions, are inconsistent with compositions plotting within the alkali basalts field on a total alkali-silica diagram (Fig. 6a), suggesting major element chemistry has also been changed. These secondary processes may have occurred on or under the seafloor, during subduction and metamorphism or after emplacement in the crust. The wide range in Sr isotope ratios at constant $\varepsilon_{Nd}(t)$ values (Fig. 7), however, strongly suggests that at least some of the chemical disturbances occurred through reaction with seawater prior to the eclogite-facies metamorphism. Thus, only the immobile elements and Nd isotopes are considered in the following discussion.

In their earlier study, Zhai et al. (2011b) classified the Pianshishan eclogites as oceanic eclogites, i.e., their protoliths formed in the oceanic crust, and proposed that their protoliths were similar to the modern OIB and had been generated within the Paleo-Tethys Ocean. Furthermore, based on their occurrence in association with marbles and garnet-phengite schists, Zhai et al. (2011a) suggested the protoliths formed as a seamount on oceanic crust. The results presented here are entirely consistent with this interpretation: the Nd isotopic compositions are similar to the OIB, as are their trace element characteristics. The zircon O isotope compositions as well as positive rather than negative Ta and Nb anomalies indicate a lack of a significant sediment or continental component. All of these observations are consistent with their generation as intraplate oceanic basalts, including those occurring on seamounts.

REE modeling suggests that the protoliths were generated by relatively low melt fractions and the HREE depletion indicates melting occurred below the garnet-spinel transition zone (Fig. 9). Based on the trace element patterns and Nd isotopic signatures that are slightly enriched relative to the mid-ocean ridge basalts (MORB), we infer the original basaltic rocks were produced by partial melting of oceanic asthenospheric mantle similar to the OIB sources. Although OIB are

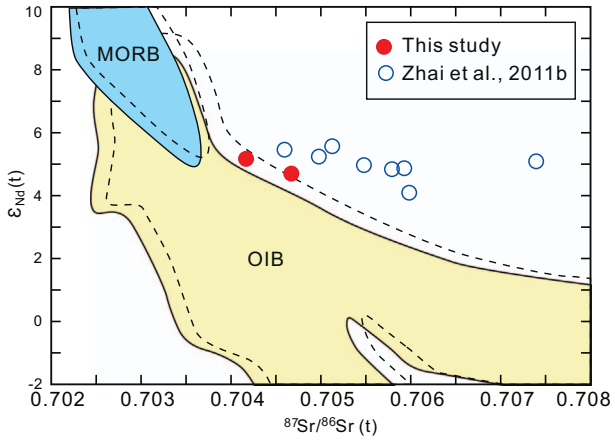

Fig. 7. Plot of Sr-Nd isotopes for the Pianshishan eclogites. Dashed lines outline fields for modern mid-ocean ridge basalts (MORB) and OIB based on (White, 2015). Solid lines outline fields calculated for ~238 Ma MORB and OIB, respectively, assuming $^{87}Rb/^{86}Sr$ between 0.0465 and 0.121 and $^{147}Sm/^{144}Nd$ between 0.1212 and 0.213 for the OIB mantle, and $^{87}Rb/^{86}Sr$ between 0.039 and 0.054 and $^{147}Sm/^{144}Nd$ between 0.205 and 0.214 for the MORB mantle.

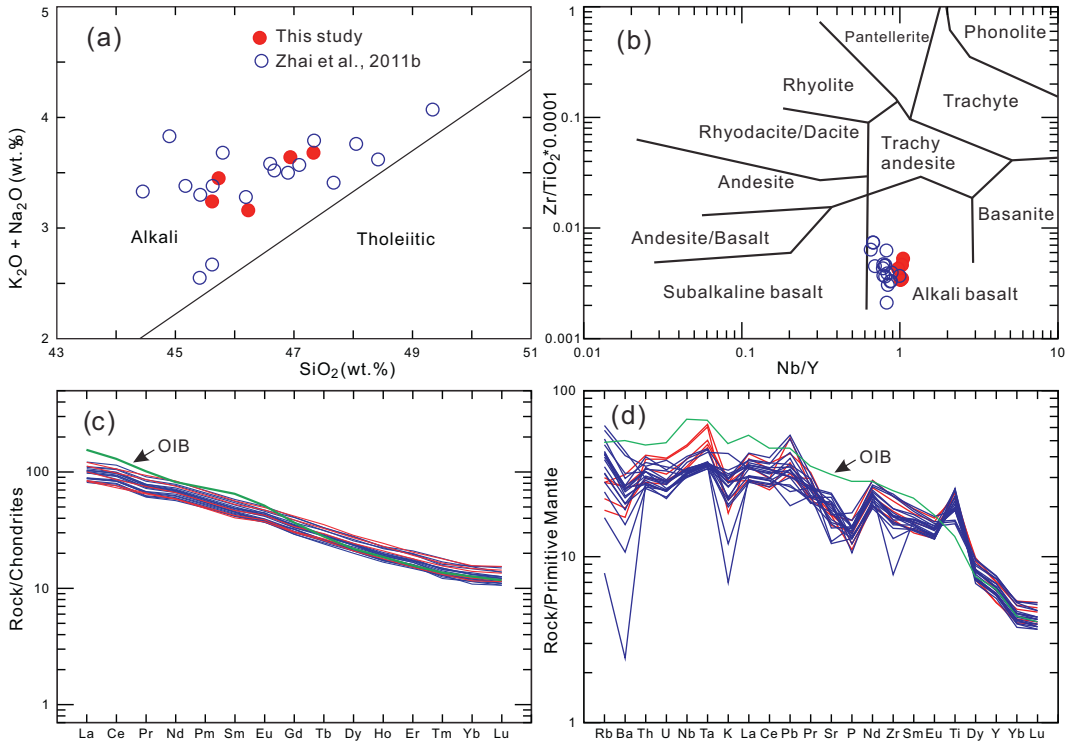

Fig. 6. (a) SiO_2 vs. $K_2O + Na_2O$ (MacDonald and Katsura, 1964); (b) Nb/Y vs. Zr/TiO_2 (Winchester and Floyd, 1977); (c) Chondrite-normalized REE distribution patterns; (d) Primitive mantle-normalized incompatible trace element spidergrams (normalization and OIB values from Sun and McDonough, 1989) for the Pianshishan eclogites.

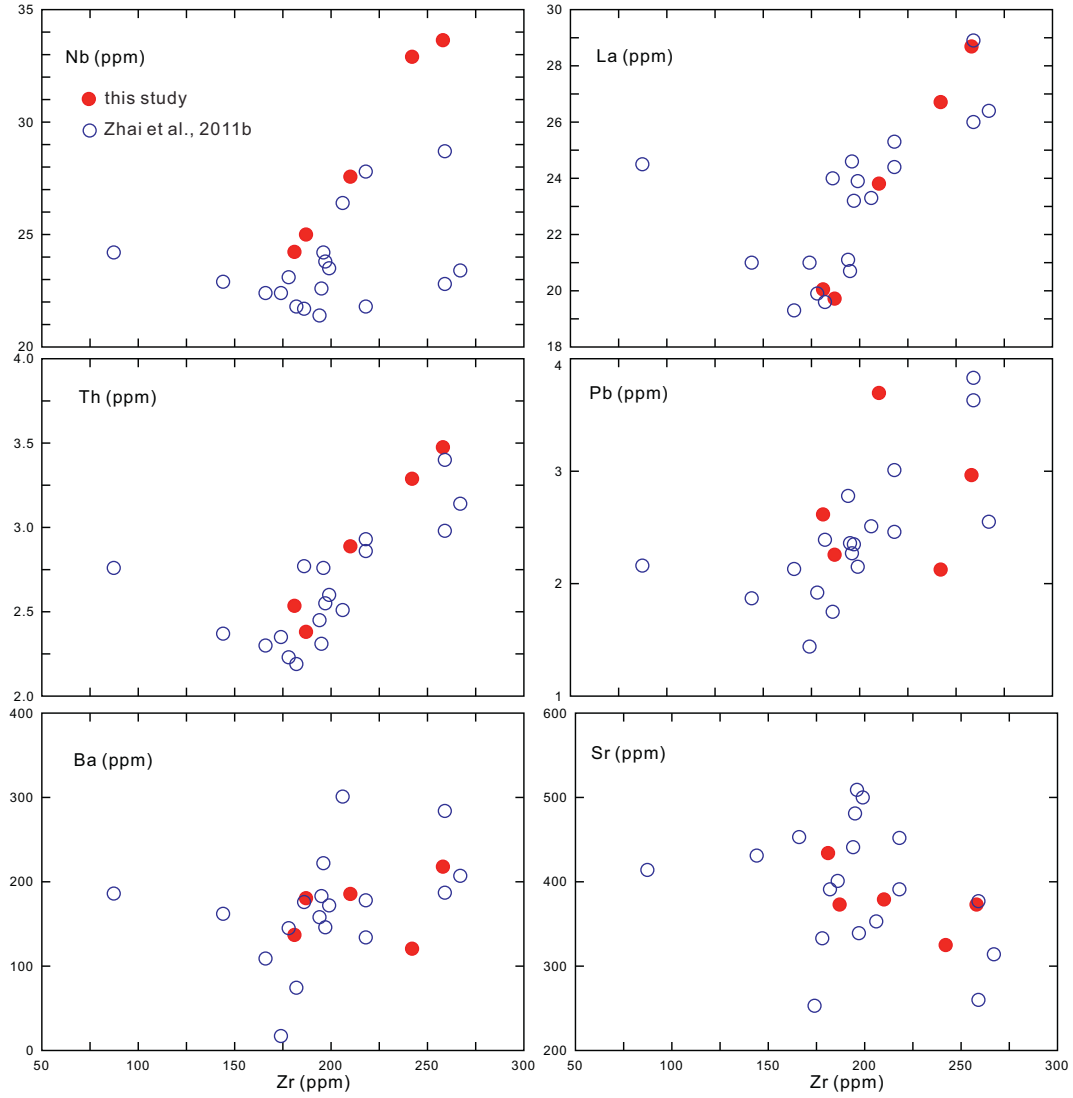

Fig. 8. Plots of selected elements versus Zr to evaluate the mobility of these elements. The Nb,Th, and rare earths appear immobile in our data while the Sr, Ba, and Pb do not.

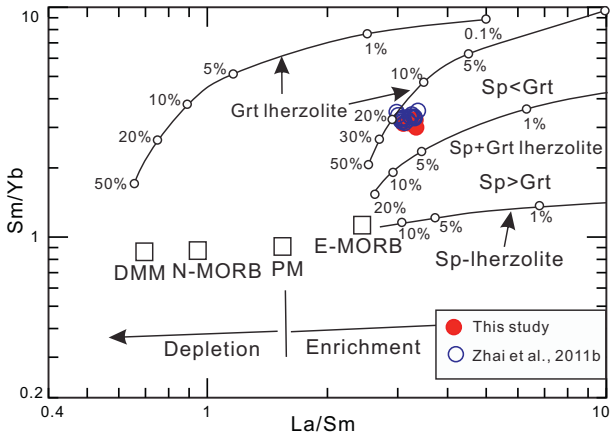

Fig. 9. Calculated paths of La/Sm and Sm/Yb during partial melting in the garnet and spinel lherzolitestability fields (Aldanmaz et al., 2000). Numbers refer to percentages of melts. Also shown are the compositions of depleted MORB mantle(DMM), normal MORB (NMORB), enriched MORB (EMORB) and primitive mantle (PM).

often the products of mantle plumes, the modern ocean floor is littered with seamounts, many if not most of which are chemically similar to the OIB, yet are not associated with plumes. Instead, they are likely products of melting of incompatible enriched heterogeneities within the upper oceanic asthenospheric mantle. Many seamounts were apparently also present in the Paleo-Tethys Ocean (Zhang et al., 2006b) and we suggest that Pianshishan protoliths originated as one such seamount, consistent with the earlier inference of Zhai et al. (2011a, 2011b).

As discussed below, the inferred seamount likely formed close to the Longmu Co-Shuanghu subduction zone, raising the question of whether the magmatism might be related to subduction. Hirano et al. (2006) reported small (< 1 km^3) and young (< 8 My) volcanoes within a few kilometers of the Japan Trench. The volcanoes consist of small melt fraction alkali basalts and formed as a result of the ~800 m upward flexure that forms the "outer rise" of the Pacific Plate just prior to subduction. Hirano et al. (2006) called this "petit-spot" volcanism, in contrast to more common and voluminous hot spot volcanism. Given their alkali, incompatible element-enriched nature, we suggest that the protoliths of the Pianshishan eclogites may be a Triassic example of such "petit-spot" volcanism.

5.3. Rapid formation of the eclogite within 5 My from basalt generation

In the previous study of Pullen et al. (2008), imprecise Lu-Hf dates of 244 ± 11 and 233 ± 13 Ma were interpreted as the timing of eclogite-facies metamorphism of the Pianshishan eclogites. These dates

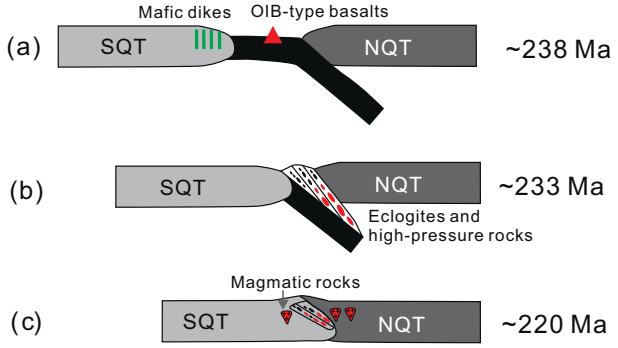

Fig. 10. Cartoon illustrating the rapid formation of the Pianshishan eclogites. (a) Generation of mafic dikes emplaced on northern margin of the SQT (Dan et al., under review) and OIB-like Pianshishan eclogite protoliths emplaced as a seamount in a nearly closed Paleo-Tethys Ocean at ~238 Ma; (b) formation of the Pianshishan eclogites and collision of the SQT and NQT at ~233 Ma; (c) exhumation of the Pianshishan eclogites to middle to upper crust at ~220 Ma and the post-collision magmatic "flare-up" at ~225–205 Ma.

are within error of the protolith formation age (~238 Ma) we report here. But the large uncertainty, probably reflecting the low $^{176}Lu/^{177}Hf$ ratios (< 0.15) and/or long growth history of garnets (Lapen et al., 2003), indicates that they should be used with caution. Thus, we tentatively consider the eclogite-facies metamorphic age to be the lower of these values, 233 Ma.

The $^{40}Ar/^{39}Ar$ dates of 220–214 Ma for the Pianshishan eclogites were interpreted to be the time the phengites, which formed during peak metamorphism (482–625 °C, Zhang et al., 2006a; or 410–460 °C, Zhai et al., 2011a), cooled through the closure temperature of 350–400 °C during the retrograde metamorphism (Zhai et al., 2011a). This implies an exhumation rate of 2.6–5.1 mm/yr (peak metamorphism of 2.0–2.5 GPa at 233 Ma and exhumed to 0.5 GPa at 220–214 Ma), which is similar to many other oceanic eclogites with exhumation rates of 1–5 mm/yr (Agard et al., 2009). The exhumation ages also serve as a minimum age for the collision between the SQT and NQT and closure of the Paleo-Tethys Ocean.

Recently, 239 Ma mafic dike swarms were discovered on the northern margin of the SQT (Fig. 1b; Dan et al., under review). Their geometry is consistent with regional extension and they were coeval with the deposition of the Songpan-Ganze flysch in an extensional back-arc basin. These features likely resulted from slab pull associated with of the Longmu Co-Shuanghu Paleo-Tethys Ocean slab. The presence of extensional rather than compressional forces at this time implies that the Paleo-Tethys Ocean had not yet closed, thus the emplacement age of these dikes and the eruption of the eclogite protoliths at ~238 Ma on the ocean floor together provide an upper limit on the age of the suture of the NQT and SQT (the LSS).

We interpret the 233 Ma peak metamorphic age of the Pianshishan eclogites as the collision of the SQT and NQT and closure of the Longmu Co-Shuanghu Paleo-Tethys Ocean. It is reasonable to assume that the peak metamorphic time was when subduction ceased, and is bracketed by the minimum and maximum ages as discussed above. This suggestion is also consistent with the peak metamorphic time being older than the post-collision magmatic "flare-up" at ~225–205 Ma documented by Wu et al. (2015).

In summary, the Pianshishan eclogites underwent a rapid cycle from generation in the oceanic crust (~238 Ma), subduction to a depth of ~65–80 km (~233 Ma), and exhumation into shallow crust (~220 Ma) within 18 My (Fig. 10). This scenario is rare and is likely due to the basaltic rocks being generated shortly before the ocean's final closure. But it does not mean that the oceanic crust is warm and young. The Early Carboniferous and Early Permian ophiolites discovered in the Longmu Co-Shuanghu suture zone (Zhang X.Z. et al., 2016) suggests that the oceanic crust was likely cold and old during the ocean's closure. This is not inconsistent with "petit-spot" origin proposed above, as modern examples occur on quite old Pacific crust (Hirano et al., 2006). By analogy to the modern petit-spot volcanoes, we suggest volcanoes comprising the Pianshishan eclogites were small (< 1–2 km tall) and hence readily subducted (Cloos, 1993). Assuming subduction rates were at least as rapid as exhumation rates, which are often an order of magnitude higher (Agard et al., 2009), we infer subduction rates in central Qiangtang of > 2.6–5.1 cm/yr based on the 2.6–5.1 mm/yr exhumation rates we estimated above. Some 130–255 km of the oceanic crust would have been subducted over 5 My at this rate. Assuming this subduction rate was constant over the period from the protolith generation to eclogite-facies metamorphism at ~65–80 km depth and the subduction angle of 45°, this would place the ~238 Ma seamount only about 16–160 km from the trench, indicating the Paleo-Tethys Ocean had nearly closed at this time.

The eclogites with high exhumation rates (≥ cm/yr) usually have phengite $^{40}Ar/^{39}Ar$ ages similar to the metamorphic zircon ages, such as the eclogites of the Kaghan Valley, Pakistan (Wilke et al., 2010a, 2010b). However, the $^{40}Ar/^{39}Ar$ dates of 220–214 Ma of the Pianshishan eclogites (Li et al., 2006b; Zhai et al., 2011a) are younger than the zircon U-Pb dates of ~238 Ma, although the whole cycle from protolith formation to exhumation was fast. This difference is ascribed to the lack of metamorphic zircons or rims in the Pianshishan eclogites and all of the zircons being of igneous origin. Thus, their zircon dates, representing the crystallization time of their protoliths, should be older than the $^{40}Ar/^{39}Ar$ cooling ages of the phengite from eclogites. In addition, both the calculated exhumation rates (2.6–5.1 mm/yr) and proposed subduction rates (2.6–5.1 cm/yr) for the Pianshishan eclogites are low and comparable to other oceanic eclogites (Agard et al., 2009), and the fast cycle is attributed to the eclogite protoliths being generated near the trench as discussed above.

6. Conclusions

Several lines of evidence demonstrate that the zircons in the Pianshishan eclogites were of primary igneous origin and their date of ~238 Ma represents the formation age of the protolith. They are geochemically similar to the OIB and were probably generated by small extents partial melting of oceanic asthenospheric mantle within the garnet stability zone. This is consistent with the earlier interpretation of Zhai et al. (2011b) that they were emplaced or erupted as a seamount on oceanic crust. The protoliths of the Pianshishan eclogites were metamorphosed to eclogites-facies grade at ~233 Ma, which marks the timing of collision between the Southern Qiangtang and Northern Qiangtang terranes. This rapid evolution from basalt generation to eclogite-facies metamorphism within 5 My is due to their formation near the trench, perhaps analogous to the "petit-spot" volcanoes formed on the Japan Trench outer rise (Hirano et al., 2006).

Acknowledgments

We thank Hao Cheng for discussion in the Lu-Hf dates interpretation. Thoughtful and constructive comments by Editor-in Chief Dr. Klaus Mezger and two anonymous reviewers substantially improved the manuscript. This study was supported by the National Key R & D Program of China (2016YFC0600407), the National Natural Science Foundation of China (grant nos. 41573027 and 41630208), the Key Program of the Chinese Academy of Sciences (QYZDJ-SSW-DQC026), the Talent Project of Guangdong Province (2014TX01Z079), the Guangzhou Institute of Geochemistry, Chinese Academy of Sciences (GIGCAS 135 Project [135TP201601]), and the China Scholarship. This is contribution No. IS-2483 from GIGCAS.

References

Agard, P., Yamato, P., Joliver, L., Burov, E., 2009. Exhumation of oceanic blueschists and

eclogites in subduction zones: timing and mechanisms. Earth Sci. Rev. 92, 53–79.
Aldanmaz, E., Pearce, J.A., Thirlwall, M.F., Mitchell, J.G., 2000. Petrogenetic evolution of late Cenozoic, post-collision volcanism in western Anatolia, Turkey. J. Volcanol. Geotherm. Res. 102, 67–95.
Boehnke, P., Watson, E.B., Trail, D., Harrison, T.M., Schmitt, A.K., 2013. Zircon saturation re-revisited. Chem. Geol. 351, 324–334.
Chen, R.X., Zheng, Y.F., Xie, L.W., 2010. Metamorphic growth and recrystallization of zircon: distinction by simultaneous in-situ analyses of trace elements, U–Th–Pb and Lu–Hf isotopes in zircons from eclogite-facies rocks in the Sulu orogen. Lithos 114, 132–154.
Cheng, H., Liu, Y.M., Vervoort, J.D., Lu, H.H., 2015. Combined U-Pb, Lu-Hf, Sm-Nd and Ar-Ar multichronometric dating on the Bailang eclogite constrains the closure timing of the Paleo-Tethys Ocean in the Lhasa terrane, Tibet. Gondwana Res. 28, 1482–1499.
Cloos, M., 1993. Lithospheric buoyancy and collisional orogenesis - subduction of oceanic plateaus, continental margins, island arcs, spreading ridges, and seamounts. Geol. Soc. Am. Bull. 105, 715–737.
Corfu, F., Hanchar, J.M., Hoskin, P.W.O., Kinny, P., 2003. Altas of zircon textures. In: Hanchar, J.M., Hoskin, P.W.O. (Eds.), Zircon: Chantilly Virginia, Reviews in Mineralogy and Geochemistry. 53. pp. 469–500.
Dan, W., Wang, Q., White, W.M., Li, X.H., Zhang, X.Z., Tang, G.J., Jiang, Z.Q., Ou, Q., Hao, L.L., Qi, Y., 2017. Triassic Passive Margin Magmatism in Central Tibet Caused By Slab Pull. under review.
Dong, Y.S., Li, C., 2009. Discovery of eclogite in the Guoganjianian Mountain, central Qiangtang area, northern Tibet, China (in Chinese with English abstract). Geol. Bull. China 28, 1197–1200.
Ferry, J.M., Watson, E.B., 2007. New thermodynamic models and revised calibrations for the Ti-in-zircon and Zr-in-rutile thermometers. Contrib. Mineral. Petrol. 154, 429–437.
Fu, B., Page, F., Cavosie, A., Fournelle, J., Kita, N., Lackey, J., Wilde, S., Valley, J., 2008. Ti-in-zircon thermometry: applications and limitations. Contrib. Mineral. Petrol. 156, 197–215.
Gebauer, D., Schertl, H.P., Brix, M., Schreyer, W., 1997. 35 Ma old ultrahigh-pressure metamorphism and evidence for very rapid exhumation in the Dora Maira Massif, western Alps. Lithos 41, 5–24.
Hirano, N., Takahashi, E., Yamamoto, J., Abe, N., Ingle, S.P., Kaneoka, I., Hirata, T., Kimura, J.-I., Ishii, T., Ogawa, Y., Machida, S., Suyehiro, K., 2006. Volcanism in response to plate flexure. Science 313, 1426–1428. http://dx.doi.org/10.1126/science.1128235.
Hoskin, P.W.O., Schaltegger, U., 2003. The composition of zircon and igneous and metamorphic petrogenesis. In: Hanchar, J.M., Hoskin, P.W.O. (Eds.), Zircon: Chantilly Virginia, Reviews in Mineralogy and Geochemistry. 53. pp. 27–62.
Jiang, Q.Y., Li, C., Su, L., Hu, P.Y., Xie, C.M., Wu, H., 2015. Carboniferous arc magmatism in the Qiangtang area, northern Tibet: zircon U–Pb ages, geochemical and Lu–Hf isotopic characteristics, and tectonic implications. J. Asian Earth Sci. 100, 132–144.
Lapen, T.J., Johnson, C.M., Baumgartner, L.P., Mahlen, N.J., Beard, B.L., Amato, J.M., 2003. Burial rates during prograde metamorphism of an ultra-high-pressure terrane: an example from Lago di Cignana, western Alps, Italy. Earth Planet. Sci. Lett. 2003, 57–72.
Lee, J.K.W., Williams, I.S., Ellis, D.J., 1997. Pb, U and Th diffusion in natural zircon. Nature 390 (6656), 159–162. http://dx.doi.org/10.1038/36554.
Li, C., 1987. The Longmu Co-Shuanghu-Lanchangjiang plate suture and the north boundary of distribution of Gondwana affinity Permian-Carboniferous system in northern Tibet, China (in Chinese with English abstract). J. Changchun Univ. Earth Sci. 17, 155–166.
Li, X.H., Sun, M., Wei, G.J., Liu, Y., Lee, C.Y., Malpas, J.G., 2000. Geochemical and Sm–Nd isotopic study of amphibolites in the Cathaysia Block, SE China: evidence for extremely depleted mantle in the Paleoproterozoic. Precambrian Res. 102, 251–262.
Li, X.H., Liu, D.Y., Sun, M., Li, W.X., Liang, X.R., Liu, Y., 2004. Precise Sm-Nd and U-Pb isotopic dating of the supergiant Shizhuyuan polymetallic deposit and its host granite, SE China. Geol. Mag. 141, 225–231.
Li, X.H., Qi, C.S., Liu, Y., Liang, X.R., Tu, X.L., Xie, L.W., Yang, Y.H., 2005. Petrogenesis of the Neoproterozoic bimodal volcanic rocks along the western margin of the Yangtze Block: new constraints from Hf isotopes and Fe/Mn ratios. Chin. Sci. Bull. 50, 2481–2486.
Li, C., Zhai, Q.G., Dong, Y.S., Huang, X.P., 2006a. Discovery of eclogite and its geological significance in Qiangtang area, central Tibet. Chin. Sci. Bull. 51, 1095–1100.
Li, C., Zhai, Q.G., Chen, W., Yu, J.J., Huang, X.P., Zhang, Y., 2006b. Ar–Ar chronometry of the eclogite from central Qiangtang area, Qinghai-Tibet Plateau (in Chinese with English abstract). Acta Petrol. Sin. 22, 2843–2849.
Li, X.H., Liu, Y., Li, Q.L., Guo, C.H., Chamberlain, K.R., 2009. Precise determination of Phanerozoic zircon Pb/Pb age by multicollector SIMS without external standardization. Geochem. Geophys. Geosyst. 10, Q04010. http://dx.doi.org/10.1029/2009GC002400.
Li, Q.L., Li, X.H., Liu, Y., Tang, G.Q., Yang, J.H., Zhu, W.G., 2010. Precise U-Pb and Pb-Pb dating of Phanerozoic baddeleyite by SIMS with oxygen flooding technique. J. Anal. At. Spectrom. 25, 1107–1113.
Li, X.H., Li, W.X., Li, Q.L., Wang, X.C., Liu, Y., Yang, Y.H., 2010a. Petrogenesis and tectonic significance of the similar to 850 Ma Gangbian alkaline complex in South China: evidence from in situ zircon U-Pb dating, Hf-O isotopes and whole-rock geochemistry. Lithos 114, 1–15.
Li, X.H., Long, W.G., Li, Q.L., Liu, Y., Zheng, Y.F., Yang, Y.H., Chamberlain, K.R., Wan, D.F., Guo, C.H., Wang, X.C., Tao, H., 2010b. Penglai zircon megacrysts: a potential new working reference material for microbeam determination of Hf-O isotopes and U-Pb age. Geostand. Geoanal. Res. 34, 117–134.
Li, X.H., Tang, G.Q., Gong, B., Yang, Y.H., Hou, K.J., Hu, Z.C., Li, Q.L., Liu, Y., Li, W.X., 2013. Qinghu zircon: a working reference for microbeam analysis of U-Pb age and Hf and O isotopes. Chin. Sci. Bull. 58, 4647–4654.
Macdonald, G.A., Katsura, T., 1964. Chemical composition of Hawaiian lavas. J. Petrol. 5, 82–133.
Metcalfe, I., 1996. Gondwanaland dispersion, Asian accretion and evolution of eastern Tethys. Aust. J. Earth Sci. 43, 605–623.
Metcalfe, I., 2013. Gondwana dispersion and Asian accretion: tectonic and palaeogeographic evolution of eastern Tethys. J. Asian Earth Sci. 66, 1–33.
Möller, A., O'Brien, P.J., Kennedy, A., Kroner, A., 2003. Linking growth episodes of zircon and metamorphic textures to zircon chemistry: an example from the ultra-high temperature granulites of Rogaland (SW Norway). Eur. Mineral. UnionNotes Mineral. 5, 65–82.
Pullen, A., Kapp, P., Gehrels, G.E., Vervoort, J.D., Ding, L., 2008. Triassic continental subduction in central Tibet and Mediterranean-style closure of the Paleo-Tethys Ocean. Geology 36, 351–354.
Sun, S.S., McDonough, W.F., 1989. Chemical and isotopic systematics of oceanic basalt: implications for mantle composition and processes. In: Sanders, A.D., Norry, M.J. (Eds.), Magmatism in the Ocean Basins. Geological Society Special Publication 42. pp. 528–548.
Tang, G.Q., Li, X.H., Li, Q.L., Liu, Y., Ling, X.X., Yin, Q.Z., 2015. Deciphering the physical mechanism of the topography effect for oxygen isotope measurements using a Cameca IMS-1280 SIMS. J. Anal. At. Spectrom. 30, 950–956.
Valley, J.W., Kinny, P.D., Schulze, D.J., Spicuzza, M.J., 1998. Zircon megacrysts from kimberlite: oxygen isotope variability among mantle melts. Contrib. Mineral. Petrol. 133, 1–11.
White, W.M., 2015. Probing the earth's deep interior through geochemistry. Geochem. Perspect. 4, 95–251. http://dx.doi.org/10.7185/geochempersp.4.2.
Wiedenbeck, M., Hanchar, J.M., Peck, W.H., Sylvester, P., Valley, J., Whitehouse, M., Kronz, A., Morishita, Y., Nasdala, L., Fiebig, J., Franchi, I., Girard, J.P., Greenwood, R.C., Hinton, R., Kita, N., Mason, P.R.D., Norman, M., Ogasawara, M., Piccoli, R., Rhede, D., Satoh, H., Schulz-Dobrick, B., Skar, O., Spicuzza, M.J., Terada, K., Tindle, A., Togashi, S., Vennemann, T., Xie, Q., Zheng, Y.F., 2004. Further characterisation of the 91500 zircon crystal. Geostand. Geoanal. Res. 28, 9–39.
Wilke, F.D.H., O'Brien, P.J., Altenberger, U., Konrad-Schmolke, M., Khan, M.A., 2010a. Multi-stage reaction history in different eclogite types from the Pakistan Himalaya and implications for exhumation processes. Lithos 114, 70–85.
Wilke, F.D.H., O'Brien, P.J., Gerdes, A., Timmerman, M.J., Sudo, M., Khan, M.A., 2010b. The multistage exhumation history of the Kaghan Valley UHP series, NW Himalaya, Pakistan from U-Pb and $^{40}Ar/^{39}Ar$ ages. Eur. J. Mineral. 22, 703–719.
Winchester, J.A., Floyd, P.A., 1977. Geochemical discrimination of different magma series and their differentiation products using immobile elements. Chem. Geol. 20, 325–343.
Wu, Y.B., Zheng, Y.F., 2004. Genesis of zircon and its constraints on interpretation of U-Pb age. Chin. Sci. Bull. 49, 1554–1569.
Wu, H., Li, C., Chen, J.W., Xie, C.M., 2015. Late Triassic tectonic framework and evolution of Central Qiangtang, Tibet, SW China. Lithosphere 8, 141–149.
Xie, L.W., Zhang, Y.B., Zhang, H.H., Sun, J.F., Wu, F.Y., 2008. In situ simultaneous determination of trace elements, U–Pb and Lu–Hf isotopes in zircon and baddeleyite. Chin. Sci. Bull. 53, 1565–1573.
Yang, T.N., Ding, Y., Zhang, H.R., Fan, J.W., Liang, M.J., Wang, X.H., 2014. Two-phase subduction and subsequent collision defines the Paleotethyan tectonics of the southeastern Tibetan Plateau: evidence from zircon U-Pb dating, geochemistry, and structural geology of the Sanjiang orogenic belt, southwest China. Geol. Soc. Am. Bull. 126, 1654–1682.
Yin, A., Harrison, T.M., 2000. Geologic evolution of the Himalayan–Tibetan orogen. Annu. Rev. Earth Planet. Sci. 28, 211–280.
Zhai, Q.G., Zhang, R.Y., Jahn, B.M., Li, C., Song, S.G., Wang, J., 2011a. Triassic eclogites from central Qiangtang, northern Tibet, China: petrology, geochronology and metamorphic P-T path. Lithos 125, 173–189.
Zhai, Q.G., Jahn, B.M., Zhang, R.Y., Wang, J., Su, L., 2011b. Triassic Subduction of the Paleo-Tethys in northern Tibet, China: evidence from the geochemical and isotopic characteristics of eclogites and blueschists of the Qiangtang Block. J. Asian Earth Sci. 42, 1356–1370.
Zhai, Q.G., Jahn, B.M., Su, L., Ernst, R.E., Wang, K.L., Zhang, R.Y., Wang, J., Tang, S.H., 2013. SHRIMP zircon U–Pb geochronology, geochemistry and Sr–Nd–Hf isotopic compositions of a mafic dike swarm in the Qiangtang terrane, northern Tibet and geodynamic implications. Lithos 174, 28–43.
Zhang, K.J., Cai, J.X., Zhang, Y.X., Zhao, T.P., 2006a. Eclogites from central Qiangtang, northern Tibet (China) and tectonic implications. Earth Planet. Sci. Lett. 245, 722–729.
Zhang, K.J., Zhang, Y.X., Zhu, Y.T., Wei, R.Z., 2006b. The blueschist-bearing Qiangtang metamorphic belt (northern Tibet, China) as an in situ suture zone: evidence from geochemical comparison with the Jinsa suture. Geology 34, 493–496.
Zhang, Z.M., Schertl, H.P., Wang, J.L., Shen, K., Liou, J.G., 2009. Source of coesite inclusions within inherited magmatic zircon from Sulu UHP rocks, eastern China, and their bearing for fluid–rock interaction and SHRIMP dating. J. Metamorph. Geol. 27, 317–333.
Zhang, X.Z., Dong, Y.S., Li, C., Cheng, W., Shi, J.R., Zhang, Y., Wang, Y.S., 2010. Identification of the eclogites with different ages and their tectonic significance in central Qiangtang, Tibetan Plateau: constraints from $^{40}Ar/^{39}Ar$ geochronology (in Chinese with English abstract). Geol. Bull. China 29, 1815–1824.
Zhang, X.Z., Dong, Y.S., Wang, Q., Dan, W., Zhang, C.F., Deng, M.R., Xu, W., Xia, X.P., Zeng, J.P., Ling, H., 2016. Carboniferous and Permian evolutionary records for the Paleo-Tethys Ocean constrained by newly discovered Xiangtaohu ophiolites from central Qiangtang, central Tibet. Tectonics 35. http://dx.doi.org/10.1002/2016TC004170.
Zhang, L., Chen, R.X., Zheng, Y.F., Li, W.C., Hu, Z.C., Yang, Y.H., Tang, H.L., 2016a. The tectonic transition from oceanic subduction to continental subduction: Zirconological constraints from two types of eclogites in the North Qaidam orogen, northern Tibet. Lithos 244, 122–139.
Zhang, L., Chen, R.X., Zheng, Y.F., Hu, Z.C., Yang, Y.H., Xu, L.J., 2016b. Geochemical constraints on the protoliths of eclogites and blueschists from North Qilian, northern Tibet. Chem. Geol. 421, 26–43.